

PPPL- 5090

PPPL-5090

## High Performance Discharges in the Lithium Tokamak eXperiment with Liquid Lithium Walls

J.C. Schmitt, R.E. Bell, D.P. Boyle, B. Esposti,  
R. Kaita, T. Kozub, B.P. LeBlanc, et al.

November 2014



# Princeton Plasma Physics Laboratory

## Report Disclaimers

---

### Full Legal Disclaimer

This report was prepared as an account of work sponsored by an agency of the United States Government. Neither the United States Government nor any agency thereof, nor any of their employees, nor any of their contractors, subcontractors or their employees, makes any warranty, express or implied, or assumes any legal liability or responsibility for the accuracy, completeness, or any third party's use or the results of such use of any information, apparatus, product, or process disclosed, or represents that its use would not infringe privately owned rights. Reference herein to any specific commercial product, process, or service by trade name, trademark, manufacturer, or otherwise, does not necessarily constitute or imply its endorsement, recommendation, or favoring by the United States Government or any agency thereof or its contractors or subcontractors. The views and opinions of authors expressed herein do not necessarily state or reflect those of the United States Government or any agency thereof.

### Trademark Disclaimer

Reference herein to any specific commercial product, process, or service by trade name, trademark, manufacturer, or otherwise, does not necessarily constitute or imply its endorsement, recommendation, or favoring by the United States Government or any agency thereof or its contractors or subcontractors.

---

## PPPL Report Availability

### Princeton Plasma Physics Laboratory:

<http://www.pppl.gov/techreports.cfm>

### Office of Scientific and Technical Information (OSTI):

<http://www.osti.gov/scitech/>

---

### Related Links:

[U.S. Department of Energy](#)

[Office of Scientific and Technical Information](#)

High performance discharges in the Lithium Tokamak eXperiment with liquid lithium walls

J.C. Schmitt, R.E. Bell, D.P. Boyle, B. Esposti, R. Kaita, T. Kozub, B.P. LeBlanc, M. Lucia, R. Maingi, R. Majeski, E. Merino, S. Punjabi-Vinoth, G. Tchilingurian  
*Princeton Plasma Physics Laboratory, Princeton, New Jersey 08543, USA*

A. Capece, B. Koel, J. Roszell  
*Princeton University, Princeton, New Jersey 08544, USA*

T. M. Biewer, T. K. Gray  
*Oak Ridge National Laboratory, Oak Ridge, Tennessee 37831, USA*

S. Kubota  
*University of California at Los Angeles, Los Angeles, California 90095, USA*

P. Beiersdorfer, K. Widman  
*Lawrence Livermore National Laboratory, Livermore, California 94550, USA*

K. Tritz  
*Johns Hopkins University, Baltimore, Maryland 21218, USA*

A liquid metal first wall for a fusion reactor has been extensively discussed. Here we report the first-ever successful operation of a tokamak with a large area (40% of the total plasma surface area) liquid lithium wall in the Lithium Tokamak eXperiment (LTX). These results were obtained with a new, electron beam-based lithium evaporation system, which can deposit a lithium coating on the wall of LTX in a five-minute period. Preliminary analyses of diamagnetic and other data for discharges operated with a liquid lithium wall indicate that confinement times increased by 10× compared to discharges with helium-dispersed solid lithium coatings. Ohmic energy confinement times with fresh lithium walls, solid and liquid, exceed several relevant scaling laws. Spectroscopic analysis of the discharges indicates that oxygen levels in the discharges run against liquid walls were significantly reduced compared to discharges operated against solid lithium walls. Tokamak operations with a full liquid lithium wall (85% of the total plasma surface area) have recently started.

## I. INTRODUCTION

A liquid lithium first wall is attractive for a fusion reactor for many reasons. The APEX study<sup>1</sup> and ALPS program<sup>2</sup> have both highlighted the benefits of liquid first walls and plasma facing components (PFCs). For example, the liquid surface is not limited by erosion, can ‘self-heal’ from damage due to large heat fluxes during disruptions, and has higher tolerance to neutron damage. In addition, a low-recycling first wall is predicted to produce improvements in tokamak discharges.<sup>3,4</sup> Analysis of the supershot plasmas on the Tokamak Fusion Test Reactor (TFTR) with lithium pellet conditioning<sup>5</sup> showed an improved global energy confinement time,  $\tau_E$ , correlated with reduced edge recycling. An increase of  $\tau_E$  on TFTR was also seen with lithium aerosol injection at the edge.<sup>6</sup> With a liquid lithium limiter and full lithium wall coatings on the vacuum vessel, the Current Drive Experiment-Upgrade (CDX-U) demonstrated the largest increase in  $\tau_E$  ever observed for an Ohmic tokamak, also correlated with its low-recycling wall.<sup>7</sup> The improvement in  $\tau_E$  was a factor of 6× better compared to discharges made before lithium coatings were applied, and a factor of 2-3× higher than ITER98P(y,1) scaling.

Liquid lithium is a natural choice for a low-recycling first wall because it can continue to retain all incident deuterium ions until the entire lithium inventory has been converted to LiD.<sup>8</sup> A low recycling wall in a steady-state fusion reactor probably requires a liquid, rather than a solid, lithium wall. In addition to CDX-U, small liquid lithium limiters have been used in several experiments<sup>9,10</sup>, but the area of the liquid lithium surface has been previously limited to a few percent of the total plasma surface area. The Lithium Tokamak eXperiment (LTX) was designed to

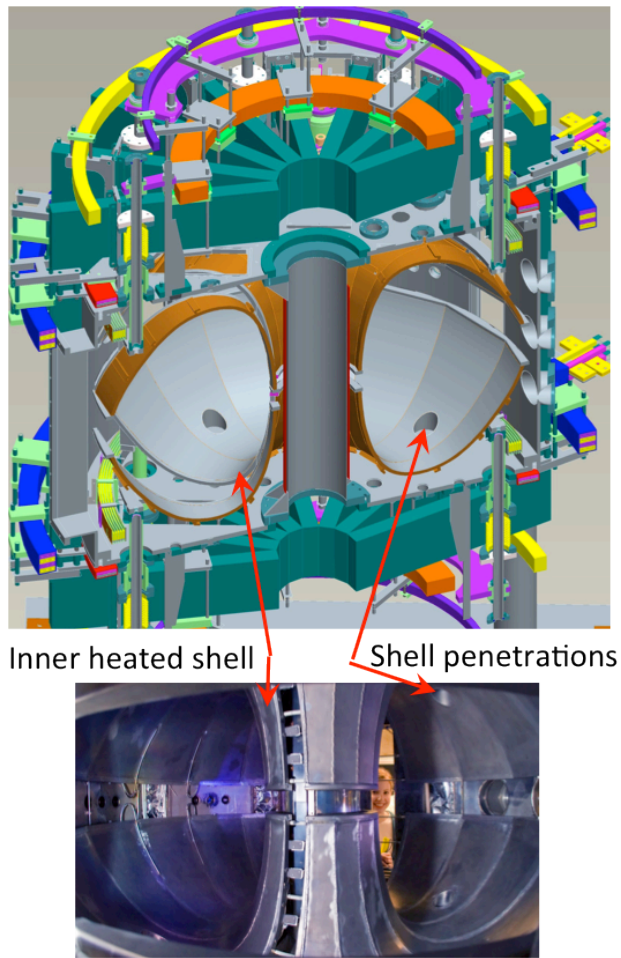
explore tokamak confinement and equilibria produced with a large-area lithium wall, either solid or liquid. Results of LTX with helium-dispersed lithium coatings have been reported previously.<sup>11</sup> Solid lithium wall coatings were shown to be beneficial for plasma performance but liquefaction of the lithium inventory resulted in large impurity influx and motivated the development of a system to produce rapid, impurity-free, lithium coatings.

In this paper, we report on results with a new method of evaporated lithium coatings produced with an electron beam. Tokamak operations with both solid and liquid lithium walls are significantly improved. This paper is organized as follows. The description of LTX is in Section II. The generation of rapid and clean lithium coatings with an electron beam (e-beam) system is described in Section III. Measurements of the impurity content and stored energy comparison are in Section IV. Section V summarizes the paper and discusses the future plans of LTX.

## II. DESCRIPTION OF LTX

The LTX tokamak is a low-aspect ratio spherical tokamak with major and minor radii of  $R_0 = 0.4$  m and  $a = 0.26$  m, respectively. The plasma elongation is  $\kappa = 1.5$ . The toroidal field on-axis is  $B_0 \approx 0.17$  T. Peak plasma currents have reached  $I_p = 75$  kA. Durations of the current flat-top have exceeded 25 ms with a reduced maximum current of  $I_p = 30$  kA. Line-averaged central densities are up to  $2 \times 10^{19} \text{ m}^{-3}$ . Central electron temperatures up to  $T_e = 200$  eV have been measured with a Thomson scattering system. Inside of the vacuum vessel, there is an inner shell, consisting of 1.5 mm of stainless steel explosively bonded to 1 cm of copper.

This shell is split into four independent and electrically isolated quadrants with toroidal and poloidal breaks between each quadrant. The plasma facing side is stainless steel and it is onto this surface that lithium coatings are evaporated. The total surface area of the shell is  $4 \text{ m}^2$  and 85% of the plasma last closed flux surface (LCFS) faces this wall. A CAD rendering of a cutaway view of LTX and a photograph of the interior of the shell is shown in Figure 1. The entire shell can be heated up to  $270 - 280 \text{ }^\circ\text{C}$  steady-state or  $350 \text{ }^\circ\text{C}$  transiently with a set of resistive heaters that are mounted on the backside of each quadrant (lithium melts at  $180.5 \text{ }^\circ\text{C}$ ). It is this heated shell that allows LTX to operate with liquid lithium wall coatings. The bottom of the shell forms a reservoir that can hold up to  $300 \text{ cm}^3$  of liquid lithium.



Inner heated shell      Shell penetrations

**Figure 1: (Color online) Top: CAD rendering of cutaway view of LTX. Bottom: Photograph of plasma confinement volume of LTX showing the inner heated shell. Two of the shell penetrations are indicated.**

### III. LITHIUM WALL COATINGS WITH ELECTRON-BEAM-HEATED LITHIUM POOLS

Previous work on LTX with helium-dispersed lithium wall coatings clearly indicated that solid, room-temperature lithium coatings were effective at reducing high-Z impurities in the plasma and reducing wall recycling.<sup>11</sup> However, liquefying the solid lithium on the LTX shell surface was not successful in creating a liquid lithium surface that would reduce recycling and sequester impurities. Heating the shell above the melting point of lithium resulted in degraded plasma performance

where the plasma stored diamagnetic energy and peak plasma current were both reduced. At the temperatures near, or above the melting point of lithium, previously absorbed impurities were released from the lithium, the plasma discharges were dominated by impurity influx, specifically oxygen, and there was increased wall recycling. This was similar to what was observed on CDX-U, when filling the tray limiter with lithium was first attempted with solid rods.<sup>12</sup> Surface coatings persisted when the tray was heated to 250 °C, which is significantly above the melting point of lithium. These results indicate the need to minimize impurity content in liquid lithium PFCs.

Dramatic improvement in plasma performance was achieved when liquid lithium walls were created in LTX with rapid lithium evaporation using the e-beam system described in this Section. This is analogous to the conditions under which significantly higher confinement times were obtained in CDX-U<sup>7</sup>. In CDX-U, liquid lithium was rapidly directed into a tray limiter from heated external reservoirs and an electron beam was used to evaporate the liquefied lithium to produce lithium coatings up to 100 nm thick on the inside of the vacuum vessel.<sup>13</sup> A similar technique is now used on LTX to rapidly evaporate clean lithium coatings onto the plasma-facing side of the inner shell. First, pieces of solid lithium are placed in a tungsten crucible that has a 9.5 mm hole in the bottom. This crucible is surrounded by a tantalum heater capable of heating the crucible to 600 °C. A tungsten plunger is placed on top of the lithium pieces to help push the liquefied lithium through the hole in the bottom of the crucible. This lithium filler system is attached to a horizontal midplane port on LTX, pumped down and then inserted into the plasma

confinement volume. The crucible is then heated well above the melting point of lithium, typically to 300 °C, the lithium liquefies and the tungsten plunger pushes the lithium out through the bottom of the crucible and onto a lower shell quadrant, where it forms a small pool. The lithium filler system is then extracted from the volume, detached from LTX, and replaced with a retractable and rotatable molybdenum mirror. A sketch of the lithium filler system and the lithium pool are shown in Figure 2. The total amount of lithium in the pool on the bottom South shell quadrant of LTX was 30 cm<sup>3</sup> for these experiments.

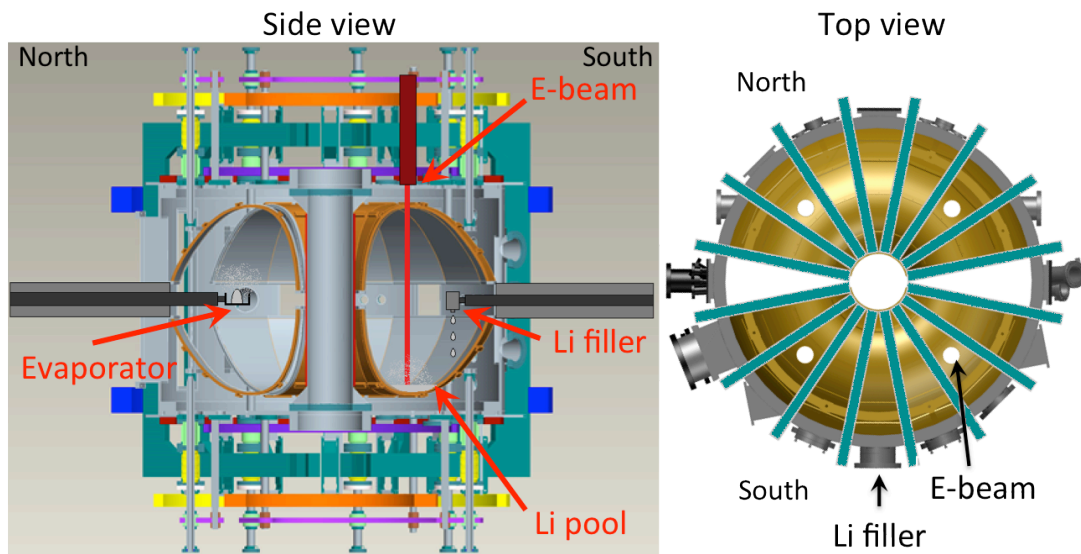


Figure 2: Sketch of an evaporator, one of the lithium fillers, lithium pools and e-beam systems on LTX.

To produce significant evaporation of lithium from the pool in a short time, the temperature of the lithium pool must be raised to 400 °C – 500 °C. The lower shell quadrant is heated to 300 °C. Next, the toroidal field coils and a subset of the poloidal field coils are used to produce a modest (~0.006 T) magnetic guide field to steer a 4 kV electron beam from a gun located at the top of the LTX vacuum vessel to the lithium pool in the lower shell, Figure 2. The e-beam is then run typically for 5

minutes at 1.2 kW – 1.5 kW output power from the gun. A molybdenum mirror provides a view of the lithium pool as it melts, stirs due to the thermoelectric effect<sup>14</sup> and evaporates. If necessary, the currents in the field coils are adjusted to ensure that the e-beam is properly aimed onto the pool and not onto the stainless steel shell.

After the evaporation cycle, the e-beam and mirror are retracted. The area of the shell coated with evaporated lithium coatings with the e-beam system is approximately 2 m<sup>2</sup>. The thickness of the evaporated coating is measured to be about 50 nm thick near the mid-plane but varies over the shell surface.<sup>15</sup> To operate with a liquid lithium wall coating, both lower and upper shell quadrants of one side of the machine are heated to 300 °C prior to the evaporation, and after the evaporation, their temperature is held constant between 270 °C and 300 °C. For experiments with solid coatings, the shells are allowed to cool after the evaporated coating is applied.

The results discussed in the paper are with lithium coatings that are primarily on the South shells of LTX (Figure 2). This is not to suggest that the North side shells have no lithium coverage. Early in the 2014 run campaign, prior to the data collected here, 15 cm<sup>3</sup> of lithium were deposited onto the bottom North shell quadrant with a filler system. No e-beam was available to heat the lithium pool on the bottom of the North shell quadrant for the data presented here. However, redeposition of evaporated and/or sputtered lithium has likely increased the total lithium inventory on the North shells. This level of redeposition is difficult to directly quantify with the current diagnostic set on LTX, but could have contributed

to the hydrogen retention and impurity control that led to the improved LTX plasma performance. Recently, a second electron beam evaporator system was installed on LTX, which allows for coating the entire shell inner surface.

#### IV. PERFORMANCE OF LTX PLASMAS WITH RAPIDLY DEPOSITIED LITHIUM WALL COATINGS

##### A. SPECTROSCOPY MEASUREMENTS

Spectroscopic measurements of plasma emission are the most reliable means to measure the level of impurities in the plasmas in LTX under various wall conditions. Plasma discharges on bare stainless steel walls, which are short in duration (<10 ms) and low current (<15 kA), have large impurity emission from oxygen and carbon. After the first lithium evaporation onto the bare stainless steel shells is performed, oxygen and carbon emissions are strongly reduced, and plasma performance is improved.

Core measurements of the VUV/XUV spectrum of lithium wall discharges were performed with a transmission grating imaging spectrometer (TGIS) coupled to a X-ray CCD camera. These results were reported previously<sup>16</sup> but are summarized here for context. The spectrum included three particular spectral lines, O V, O VI and Li III in the wavelength range of 10 nm – 20 nm. Changes in the impurity particle sources can be isolated by comparing values of the O/Li line ratios. The ratios of these lines are used because the ionization energies of these three charge states is not too dissimilar, 110 eV, 138 eV, and 113 eV, respectively, so the complex dependence of

the emission of each line on electron temperature,  $T_e$ , and the product of the electron density and particle confinement time,  $n_e\tau_p$ , can be largely eliminated. The plasma discharges on liquid lithium wall coatings show a decrease in the O/Li line ratio by an order of magnitude compared to discharges on solid lithium wall coatings. The reduction of the line ratio was clearly due to a decrease in the O VI emission, not an increase in the Li III emission, indicating that liquefied lithium walls were not increasing the lithium impurity influx into the plasma core. Furthermore, the O/Li line ratio continued to decrease throughout the run day, suggesting that a sufficiently clean liquid lithium surface continuously pumps oxygen impurities. In contrast, the O/Li line ratio increased throughout the solid lithium wall run, suggesting that oxygen was building up on the surface of the solid lithium.

A new technique to estimate lithium contamination in LTX was demonstrated using a photometrically-calibrated high-throughput visible spectrometer<sup>17</sup>. Line-integrated measurements of Li III at 450 nm along toroidal sightlines were inverted to get a local emissivity. The  $T_e$  profiles from the Thomson scattering system were fit with a  $(1 - \rho^2)^n$  parameterization, and  $T_e$ -dependent photoemission rate coefficients were calculated from the ADAS database<sup>18</sup>. The  $\text{Li}^{2+}$  concentration appears hollow, ranging from 0.05% in the core to a few percent near the edge. The hollowness is probably due to the higher  $T_e$  burning out the  $\text{Li}^{2+}$  near the core. At radii where  $\text{Li}^{2+}$  emission is most likely to be excited, the level is about 0.5-1%. If the overall lithium concentration is constant, this 0.5-1% is probably more indicative of

the overall lithium concentration in the core. Low core plasma lithium concentrations, even with extensive wall coatings, have been previously measured in NSTX<sup>19,20</sup>. NSTX, however, benefits from the impurity screening which a divertor affords, whereas LTX is wall-limited, with much weaker impurity screening. More detailed analysis of the LTX measurements will be published in the future.

## B. STORED ENERGY MEASUREMENTS

Energy confinement times are calculated with low-beta cylindrical approximations, given by:

$$\beta_{pol} = 1 + \frac{8\pi B_0 \delta\psi}{(\mu_0 I_p)^2} \quad (1a)$$

$$W = \frac{3}{2} (0.25 \mu_0 R_0 I_p^2 \beta_{pol}) \quad (1b)$$

$$\tau_{E.Exp} = W / P_{OH} \quad (1c)$$

where  $\delta\psi$  is the change in the toroidal flux measured with an externally compensated, 2-turn diamagnetic flux loop.<sup>21</sup>  $I_p$  is the net toroidal plasma current measured with a Rogowski coil that is installed internal to the vacuum vessel (to exclude measuring currents in the vessel) and surrounds the plasma.  $B_0$  is the calculated magnitude of the toroidal field on-axis, based on measurements of the current in the toroidal field coils.  $P_{OH}$  is the calculated Ohmic input power based on the measured loop voltage and measured plasma current. The low-beta cylindrical approximation is used because equilibrium reconstructions are currently not available for LTX, so there are uncertainties in  $R_0$ , various shaping factors (elongation, triangularity, etc.), and the input power. Measurements of the radiated

power are unavailable. The values reported here are averaged over a 10 ms window near the time of peak  $I_p$ , when the values of  $I_p$  and  $\delta\psi$  are slowly changing.

The energy confinement times in LTX are modest because it is a small spherical tokamak. Comparisons to various scaling laws provide a basis for evaluating the performance of plasmas with the low recycling walls in LTX. The energy confinement time for three scaling laws, ITER-89P, an L-mode scaling law<sup>22</sup>, ITER98P(y,1), an ELMy-H mode scaling law<sup>23</sup>, and neo-Alcator<sup>24</sup> are

$$\tau_E^{I89P} = 4.8 \times 10^{-3} M^{0.5} I_p^{0.85} R_0^{1.2} a^{0.3} \kappa^{0.5} n_e^{0.1} B_0^{0.2} P^{-0.5} \quad (2)$$

$$\tau_E^{I98P(y,1)} = 5.03 \times 10^{-3} M^{0.13} I_p^{0.91} R_0^{1.48} a^{0.57} \kappa^{0.72} n_e^{0.44} B_0^{0.15} P^{-0.65} \quad (3)$$

$$\tau_E^{NeoAlc} = 1.92 \times 10^{-21} R_0^{2.04} a^{1.04} n_e \quad (4)$$

In these expressions,  $M$  is the hydrogen isotope mass, and  $P$  is the absorbed power. The line-averaged density,  $n_e$  ( $10^{18} m^{-3}$ ), is measured by a single channel 1-mm microwave interferometer on LTX. For LTX,  $R_0 = 0.4$  m,  $a = 0.26$  m,  $\kappa = 1.5$ ,  $M = 1$ , and  $P \equiv P_{OH}$ . Without equilibrium reconstructions, there are uncertainties in  $R_0$ ,  $a$ ,  $\kappa$ , and  $P$ . The exponent on  $R_0$  is the largest of these terms, 1.2 for ITER-89P, 1.48 for ITER98P(y,1), and 2.04 for neo-Alcator. The exponents on  $a$  and  $\kappa$  are less than unity in ITER-89P and ITER98P(y,1), and the exponent on  $a$  is close to unity in neo-Alcator. The exponent on  $P$  is negative. The nominal design values are used for the geometric terms ( $R_0$ ,  $a$ ,  $\kappa$ ). It is likely that the plasma discharge is not filling the entire volume ( $a_{\text{exp}} < a$ ) and that the plasma is shifted inward ( $R_{0,\text{exp}} < R_0$ ), so the calculated confinement time for each of the scaling laws may be over-estimated. Also, all of the input power ( $P_{OH}$ ) is assumed to be going into the stored kinetic

energy, while it is likely that some power is going into stored magnetic energy and being lost through radiation.

These particular scaling laws are of interest because of the following reasons. NSTX Ohmic discharges approximately followed ITER-89P scaling, exceeding it by up to a factor of  $\sim 1.4^{25}$ , and Alcator C-Mod Ohmic discharges exceeded ITER-89P by up to a factor of  $\sim 1.5^{26}$ . ITER98P(y,1) produced good fits to L- and H-mode plasmas in START<sup>27</sup>, which was similar in size to LTX. Neo-Alcator scaling provides a comparison that does not depend upon input power to the plasma. Both Alcator C-Mod and START exceeded neo-Alcator scaling, but by a factor less than 2.<sup>26,27</sup>

For each scaling law, an enhancement factor, the ratio between the experimental and calculated scaling law confinement time, was calculated:

$$H_{I89P} = \frac{\tau_{E,Exp}}{\tau_E^{I89P}} \quad (5)$$

$$H_{I98P(y,1)} = \frac{\tau_{E,Exp}}{\tau_E^{I98P(y,1)}} \quad (6)$$

$$H_{NeoAlc} = \frac{\tau_{E,Exp}}{\tau_E^{NeoAlc}} \quad (7)$$

Plots of  $(\tau_{E,Exp}, H_{I89P})$  vs.  $\tau_E^{I89P}$ ,  $(\tau_{E,Exp}, H_{I98P(y,1)})$  vs.  $\tau_E^{I98P(y,1)}$ , and  $(\tau_{E,Exp}, H_{NeoAlc})$  vs.  $\tau_E^{NeoAlc}$  are shown in Figures 3-5. Plasma discharges formed with 2-month old lithium wall coatings, assumed to be well-passivated, are shown as black squares. Discharges on solid lithium wall coatings are shown as blue circles. Discharges on liquid lithium discharges are shown as red x's. Data from helium-dispersed lithium wall coatings, taken in 2012, are shown as green triangles. Plasmas formed with

passivated lithium walls approximately follow ITER-89P scaling (Figure 3). Plasma discharges on fresh, solid lithium wall coatings exceeded those with helium-dispersed wall coatings by up to an order of magnitude, and exceeded ITER-89P by up to a factor 2. For comparison, the enhancement factor over ITER-89P achieved by CDX-U, with a liquid lithium limiter and solid lithium coatings on the vacuum vessel wall, was only 1.3.<sup>28</sup>

An interesting feature with cold shells is indicated by the set of data points highlighted by the arrow. These discharges were taken on successive days with repeated lithium evaporations. The confinement time and the enhancement factor continued to increase as more lithium was being placed on the wall. The largest enhancement factors have been achieved with liquid lithium walls. The comparison to ITER-89P clearly suggest that the performance is a function of reduced wall recycling and impurity sequestration, and that wall conditioning is an important hidden variable that is not captured in the scaling law.

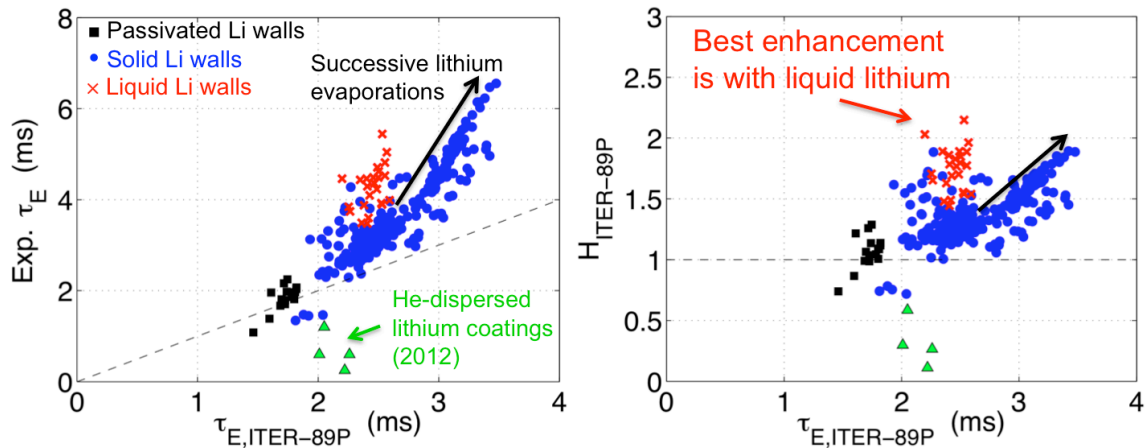


Figure 3: (Color online) Left: Experimental energy confinement time vs ITER-89P confinement scaling. Right: Enhancement factor vs ITER-89P confinement scaling.

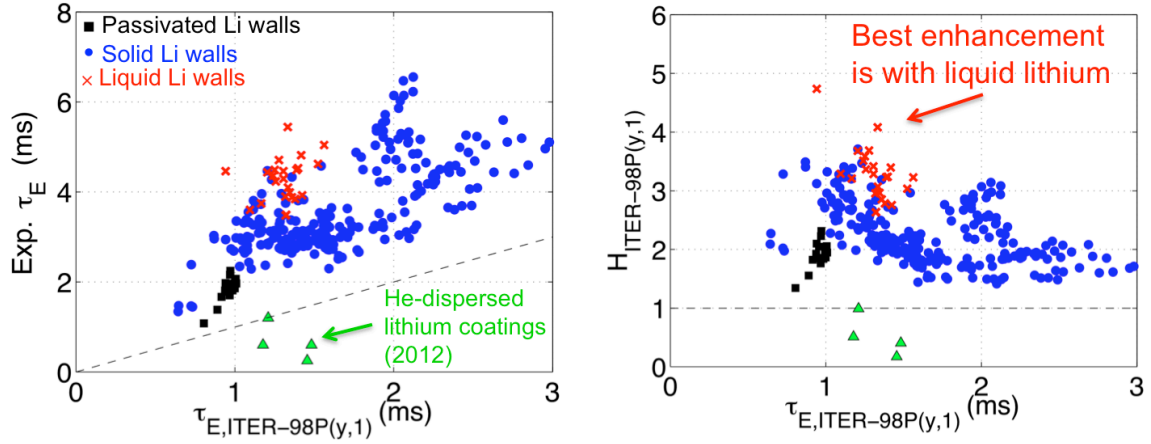


Figure 4: (Color online) Left: Experimental energy confinement time vs ITER-98P(y,1) confinement scaling. Right: Enhancement factor vs ITER-98P(y,1) confinement scaling.

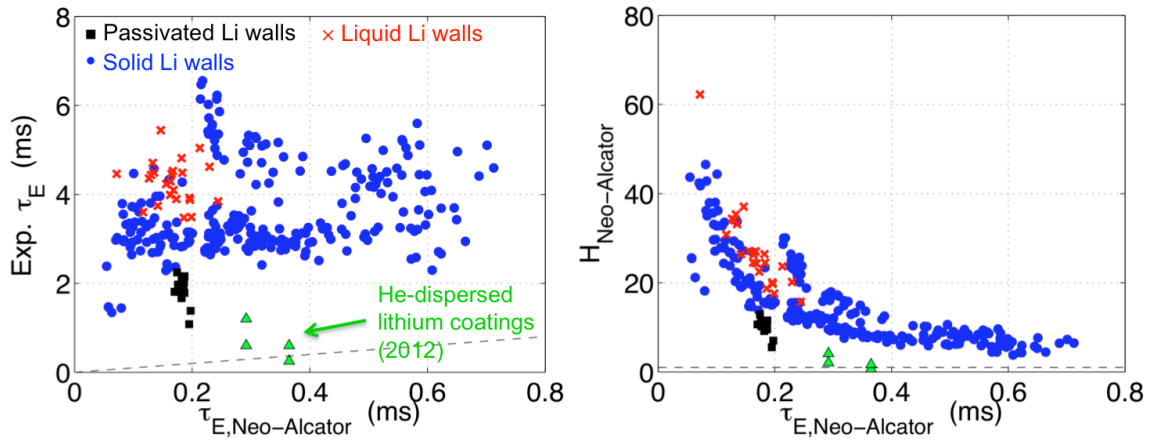


Figure 5: (Color online) Left: Experimental energy confinement time vs neo-Alcator confinement scaling. Right: Enhancement factor vs neo-Alcator confinement scaling.

The entire database of analyzed shots exceed ITER-98P(y,1) scaling, Figure 4. This represents about 90% of all plasma discharges in 2014. The largest enhancement factor over ITER-98P(y,1) achieved by CDX-U was 2.37. In LTX, with solid lithium coatings, the enhancement factors range from 1.3 to 3.7. With liquid lithium coatings the enhancement factors are somewhat higher.

Both ITER-89P and ITER-98P(y,1) scaling laws have an inverse power dependence,  $\tau_E \propto P^{-\alpha}$ . Comparing an Ohmically-heated tokamak like LTX to these scaling laws can be problematic because the input power is not an independent

variable. Neo-Alcator scaling does not scale with input power, rather it only depends on plasma size and density. As seen in Figure 5, there is no obvious density dependence for confinement in LTX discharges. The enhancement factors over neo-Alcator scaling with e-beam evaporated lithium coatings range up to ~50.

## V. SUMMARY AND FUTURE PLANS

An electron beam has been installed on LTX to heat, stir, and evaporate a lithium pool located on the bottom shell of LTX. This has led to lithium coatings that are rapidly deposited (~5 minutes), clean and free of impurities. In contrast to the liquefying of helium-dispersed lithium coatings that had been used in LTX in the past, the e-beam coatings discussed in this paper demonstrate good oxygen sequestration with liquefied lithium walls. Plasma performance with solid lithium wall coatings have also improved by an order of magnitude compared to those with helium-dispersed lithium wall coatings. Plasmas formed on 2-month old (passivated) lithium wall coatings roughly follow ITER-89P scaling. Plasmas formed on solid or liquid lithium wall exceeded all three scaling laws discussed in the paper, ITER-89P (up to ~2x), ITER-98P(y,1) (up to ~4x), and neo-Alcator (up to ~50x). The effects of wall conditioning were also highlighted as an important feature that is not captured in the scaling laws. The lithium concentration in the core is estimated to be in the 0.5-1% range, suggesting that core-contamination is not large for LTX.

The LTX and CDX-U results suggest the importance of 'fresh' surfaces when liquid lithium is used. The detailed physical and chemical properties of the lithium coatings that are responsible for hydrogen retention and impurity sequestration,

however, are not yet understood. Analysis of the measurements of the surface coatings in LTX with the Materials Analysis and Particle Probe (MAPP) are in progress<sup>29</sup> and the hydrogen retention of lithium coatings as a function of temperature and oxidation are currently under study<sup>30</sup> by the Surface Science and Technology Laboratory located at the Princeton Plasma Physics Laboratory.

Future operational plans for LTX will focus on exploring the performance of plasma discharges with all four shell quadrant heated to 270 °C with liquid lithium call coatings. A second e-beam system has been installed to heat, stir and evaporate the lithium pool on the bottom North shell quadrant. Evaporated lithium coatings form a 4 m<sup>2</sup> liquid lithium wall which 85% of the plasma LCFS faces. Good discharges have been achieved with this liquid lithium wall but are beyond the scope of this paper. An edge Thomson scattering system will characterize  $T_e$  near the lithium wall. Recycling coefficients will be quantified with DEGAS2 modeling. A bolometer, to be installed, will measure the radiated power and combined with equilibrium reconstructions<sup>31</sup> will enable accurate stored energy and energy confinement time measurement. There are also plans to acquire and install a neutral beam for core fueling.

## ACKNOWLEDGEMENTS

This work is supported by US DOE contracts DE-AC02-09CH11466 and DE-AC05-00OR22725.

- 
- <sup>1</sup> M.A. Abdou, A Ying, N. Morley, K. Gulec, S. Smolentsev, M. Kotschenreuther, S. Malang, S. Zinkle, T. Rognlien, P. Fogarty, B. Nelson, R. Nygren, K. McCarthy, M.Z. Youssef, N. Ghoniem, D. Sze, C. Wong, M. Sawan, H. Khater, R. Woolley, R. Mattas, R. Moir, S. Sharafat, J. Brooks, A. Hassanein, D. Petti, M. Tillack, M. Ulrickson, and T. Uchimoto, *Fusion Eng. Des.* **54**, 181 (2001).
- <sup>2</sup> J.N. Brooks, J.P. Allain, R. Bastasz, R. Doerner, T. Evans, A. Hassanein, R. Kaita, S. Luckhardt, R. Maingi, R. Majeski, N.B. Morley, M. Narula, T. Rognlien, D. Ruzic, R. Stubbers, M. Ulrickson, C.P.C. Wong, and A Ying, *Fusion Sci. Technol.* **47**, 669 (2005)
- <sup>3</sup> S.I. Krasheninnikov, L.E. Zakharov, and G.V. Pereverzev, *Phys. Plasmas* **10**, 1678 (2003).
- <sup>4</sup> L.E. Zakharov, N.N. Gorelenkov, R.B. White, S.I. Krasheninnikov, G.V. Pereverzev, *Fusion Eng. Des.* **72**, 149 (2004).
- <sup>5</sup> J.D. Strachan, *Nucl. Fusion* **34**, 1017 (1994).
- <sup>6</sup> D.K. Mansfield, D.W. Johnson, B. Grek, H.W. Kugel, M.G. Bell, R.E. Bell, R.V. Budny, C.E. Bush, E.D. Fredrickson, K.W. Hill, D.L. Jassby, R.J. Maqueda, H.K. Park, A.T. Ramsey, E.J. Synakowski, G. Taylor, and G.A. Wurden, *Nucl. Fusion* **41**, 1823 (2001).
- <sup>7</sup> R. Majeski, R. Doerner, T. Gray, R. Kaita, R. Maingi, D. Mansfield, J. Spaleta, V. Soukhanovskii, J. Timberlake, and L. Zakharov, *Phys. Rev. Let.* **97**, 075002 (2006).
- <sup>8</sup> M.J. Baldwin, R.P. Doerner, S.C. Luckhard, and R.W. Conn, *Nucl. Fusion* **42**, 1318 (2002).
- <sup>9</sup> S.V. Mirnov, V.B. Lazarev, S.M. Sotnikov, V.A. Evtikhin, I.E. Lyublinski, A.V. Vertkov, *Fusion Eng. Des.* **65**, 455 (2003).
- <sup>10</sup> V. Pericoli-Ridolfini, M.L. Apicella, G. Mazzitelli, O. Tudisco, R. Zagórski, *Plasma Phys. Control. Fusion* **49**, S123 (2007).
- <sup>11</sup> R. Majeski, T. Abrams, D. Boyle, E. Granstedt, J. Hare, C.M. Jacobson, R. Kaita, T. Kozub, B. LeBlanc, D.P. Lundberg, M. Lucia, E. Merino, J. Schmitt, D. Stotler, T.M. Biewer, J.M. Canik, T.K. Gray, R. Maingi, A.G. McLean, S. Kubota, W.A. Peebles, P. Beiersdorfer, J.H.T. Clementson, and K. Tritz, *Phys. Plasmas* **20**, 056103 (2013).
- <sup>12</sup> R. Kaita, R. Majeski, M. Boaz, P. Efthimion, B. Jones, D. Hoffman, H. Kugel, J. Menard, T. Munsat, A. Post-Zwicker, V. Soukhanovskii, J. Spaleta, G. Taylor, J. Timberlake, R. Woolley, L. Zakharov, M. Finkenthal, D. Stutman, G. Antar, R. Doerner, S. Luckhardt, R. Maingi, M. Maiorano, S. Smith, *Fusion Eng. Des.* **61-62**, 217 (2002).
- <sup>13</sup> R. Kaita, R. Majeski, T. Gray, H. Kugel, D. Mansfield, J. Spaleta, J. Timberlake, L. Zakharov, R. Doerner, T. Lynch, R. Maingi, and V. Soukhanovskii, *Phys. Plasmas* **14**, 056111 (2007).
- <sup>14</sup> M.A. Jaworski, T.K. Gray, M. Antonelli, J.J. Kim, C.Y. Lau, M.B. Lee, M.J. Neumann, W. Xu, and D.N. Ruzic, *Phys. Rev. Let.* **104**, 094503 (2010).
- <sup>15</sup> M. Lucia, R. Kaita, R. Majeski, F. Bedoya, J.P. Allain, T. Abrams, R.E. Bell, D.P. Boyle, M.A. Jaworski, J.C. Schmitt, *J. Nucl. Mater* (2014), *accepted*.
- <sup>16</sup> K. Tritz, R. Bell, P. Beiersdorfer, D. Boyle, J. Clemenson, M. Finkenthal, R. Kaita, T. Kozub, S. Kubota, M. Lucia, R. Majeski, E. Merino, J. Schmitt, D. Stutman, *Plasma Phys. Control. Fusion*, *Accepted*.
- <sup>17</sup> R.E. Bell, *Rev. Sci. Instrum.* **85**, 014104 (2014).
- <sup>18</sup> Summers, H. P. (2004) The ADAS User Manual, version 2.6 <http://www.adas.ac.uk>

- 
- <sup>19</sup> M. Podestà, R.E. Bell, A. Diallo, B.P. LeBlanc, F. Scotti and the NSTX Team, *Nucl. Fusion* **52**, 033008 (2012).
- <sup>20</sup> F. Scotti, V.A. Soukhanovskii, R.E. Bell, S. Gerhardt, W. Guttenfelder, S. Kaye, R. Andre, A. Diallo, R. Kaita, B.P. LeBlanc, M. Podestà, *Nucl. Fusion* **53**, 083001 (2013).
- <sup>21</sup> L.E. Zakharov and V.D. Shafranov, in *Reviews of Plasma Physics*, edited by M. A. Leontovich (Consultant Bureau, New York, 1986), Vol. 11, p. 153.
- <sup>22</sup> P.N. Yushmanov, T. Takizuka, K.S. Riedel, O.J.W.F. Kardaun, J.G. Cordey, S.M. Kaye, D.E. Post, *Nucl. Fusion* **30**, 1999 (1990).
- <sup>23</sup> ITER Physics Expert Groups on Confinement and Transport and Confinement Modelling and Database, ITER Physics Basis Editors and ITER EDA, *Nucl. Fusion* **39**, 2175 (1999).
- <sup>24</sup> R.R. Parker, M. Greenwald, S.C. Luckhardt, E.S. Marmor, M. Porkolab, and S.M. Wolfe, *Nucl. Fusion*, **225**, 1127 (1985).
- <sup>25</sup> S.M. Kaye, M.G. Bell, R.E. Bell, J. Bialek, T. Bigelow, M. Bitter, P. Bonoli, D. Darow, P. Efthimion, J. Ferron, E. Fredrickson, D. Gates, L. Grisham, J. Hosea, D. Johnson, R. Kaita, S. Kubota, H. Kugel, B. LeBlanc, R. Maingi, J. Manickam, T.K. Mau, R.J. Maqueda, E. Mazzucato, J. Menard, D. Mueller, B. Nelson, N. Nishino, M. Ono, F. Paoletti, S. Paul, Y-K.M. Peng, C.K. Phillips, R. Raman, P. Ryan, S.A. Sabbagh, M. Schaffer, C.H. Skinner, D. Stutman, D. Swain, E. Synakowski, Y. Takase, J. Wilgen, J.R. Wilson, W. Zhu, S. Zweben, A. Bers, M. Carter, B. Deng, C. Domier, E. Doyle, M. Finkenthal, K. Hill, T. Jarbo, S. Jardin, H. Ji, L. Lao, K.C. Lee, N. Luhmann, R. Majeski, S. Medley, H. Park, T. Peebles, R.I. Pinsker, G. Porter, A. Ram, M. Rensink, T. Roglien, D. Stotler, B. Stratton, G. Taylor, W. Wampler, G.A. Wurden, X.Q. Xu, L. Zeng and NSTX Team, *Phys. Plasmas* **8**, 1977 (2001).
- <sup>26</sup> I.H. Hutchinson, R. Boivin, F. Bombarda, P. Bonoli, S. Fairfax, C. Fiore, J. Goetz, S. Golovato, R. Granetz, M. Greenwald, S. Horne, A. Hubbard, J. Irby, B. LaBombard, B. Lipschultz, E. Marmor, G. McCracken, M. Porkolab, J. Rice, J. Snipes, Y. Takase, J. Terry, S. Wolfe, C. Christensen, D. Garnier, M. Graf, T. Hsu, T. Luke, M. May, A. Niemczewski, G. Tinios, J. Schachter, and J. Urbahn, *Phys. Plasmas* **1**, 1511 (1994).
- <sup>27</sup> M.J. Walsh, R.J. Akers, P.G. Carolan, N.J. Conway, Yu.N. Dnestrovskij, A.Yu. Dnestrovskij, M. Gryaznevich, I. Jenkins, R. Martin, A.W. Morris, M. Nightingale, C. Ribeiro, C. Roach, A. Sykes, M. Tournianski, *Bull. Am. Phys. Soc.* **43**, Q7Q.30 (1998).
- <sup>28</sup> Richard Majeski, *Personal Communication*.
- <sup>29</sup> M. Lucia, R. Kaita, R. Majeski, F. Bedoya, J.P. Allain, D.P. Boyle, J.C. Schmitt, and D.A. St. Onge, *Rev. Sci. Instrum.* **85**, 11D835 (2014).
- <sup>30</sup> A.M. Capece, J.P. Roszell, C.H. Skinner, B.E. Koel, *J. Nucl. Mater* (2014)  
<http://dx.doi.org/10.1016/j.jnucmat.2014.10.048>
- <sup>31</sup> J.C. Schmitt, J. Bialek, S. Lazerson, and R. Majeski, *Rev. Sci. Instrum.* **85**, 11E817 (2014).

---

# Princeton Plasma Physics Laboratory Office of Reports and Publications

Managed by  
Princeton University

under contract with the  
U.S. Department of Energy  
(DE-AC02-09CH11466)

---

P.O. Box 451, Princeton, NJ 08543  
Phone: 609-243-2245  
Fax: 609-243-2751

E-mail: [publications@pppl.gov](mailto:publications@pppl.gov)

Website: <http://www.pppl.gov>